Arabidopsis RUP2 represses UVR8-mediated flowering in non-inductive photoperiods

Adriana B. Arongaus[1], Song Chen[1], Marie Pireyre[1], Nina Glöckner[2], Vinicius C. Galvão[3], Andreas Albert[4], J. Barbro Winkler[4], Christian Fankhauser[3], Klaus Harter[2], and Roman Ulm[1,5]

[1]Department of Botany and Plant Biology, Section of Biology, Faculty of Sciences, University of Geneva, Geneva, Switzerland

[2]Department of Plant Physiology, Center for Plant Molecular Biology (ZMBP), University of Tübingen, Tübingen, Germany

[3]Center for Integrative Genomics, Faculty of Biology and Medicine, University of Lausanne, Lausanne, Switzerland

[4]Research Unit Environmental Simulation, Helmholtz Zentrum München, Neuherberg, Germany

[5]Institute of Genetics and Genomics of Geneva (iGE3), University of Geneva, Geneva, Switzerland

Corresponding author: roman.ulm@unige.ch

Running title: Repression of flowering in short days

Abstract

Plants have evolved complex photoreceptor-controlled mechanisms to sense and respond to seasonal changes in day length. This ability allows plants to optimally time the transition from vegetative growth to flowering. UV-B is an important part intrinsic to sunlight; however, whether and how it affects photoperiodic flowering has remained elusive as this part of the solar spectrum is typically not present in controlled plant growth conditions. Here, we report that genetic mutation of *REPRESSOR OF UV-B PHOTOMORPHOGENESIS 2* (*RUP2*) renders the facultative long-day plant *Arabidopsis thaliana* a day-neutral plant, specifically under light conditions that include UV-B radiation, and dependent on the UV RESISTANCE LOCUS 8 (UVR8) UV-B photoreceptor. We provide evidence that the floral repression activity of RUP2 involves direct interaction with CONSTANS, repression of this key activator of flowering, and suppression of *FLOWERING LOCUS T* transcription. RUP2 therefore functions as an essential repressor of UVR8-mediated induction of flowering under non-inductive short-day conditions, and thus provides a crucial mechanism of photoperiodic flowering control.

[*Keywords*: sun simulator; plant–environment interaction; photoperiodism; flowering; UV-B photoreceptor; UVR8; *Arabidopsis*]

Introduction

Timely and synchronous flowering is important to optimize pollination and to allow seed maturation during favorable environmental conditions. In addition to being adaptive traits for plants in natural environments, synchronous flowering and maximal seed yields are also crucial in horticulture and agricultural production systems. In recent decades, the genetic pathways and

regulatory proteins that promote flowering in response to changes in day length (photoperiod) were largely defined in the model species *Arabidopsis thaliana*, a facultative long-day plant [i.e. flowers early in long days (LD), but will eventually also flower under short days (SD)] (Song et al. 2015). Photoperiodic flowering in *Arabidopsis* is due to the suppression of flowering in SD, which is released under LD conditions. Flowering under inductive LD photoperiods is activated by the CONSTANS (CO) transcription factor, a master regulator of *FLOWERING LOCUS T* (*FT*) expression (Putterill et al. 1995; Samach et al. 2000; Turck et al. 2008; Andres and Coupland 2012; Song et al. 2015). FT is a major component of the florigen, a systemic signal that moves through the vasculature from the leaves into the apical meristem, where it induces flowering in response to the inductive photoperiod (Wigge et al. 2005; Corbesier et al. 2007; Jaeger and Wigge 2007; Mathieu et al. 2007; Turck et al. 2008; Song et al. 2015). Regulation of CO activity is complex and takes place at many different levels (Romera-Branchat et al. 2014; Song et al. 2015; Shim et al. 2017). A prominent component of this regulation under non-inductive SD conditions is CO ubiquitination during the night period by the CONSTITUTIVELY PHOTOMORPHOGENIC 1 (COP1) – SUPPRESSOR OF PHYTOCHROME A-105 (SPA) E3 ubiquitin ligase complex, followed by degradation in the 26S proteasome (Laubinger et al. 2006; Jang et al. 2008; Liu et al. 2008). Consistently, *cop1* and *spa1* plants flower early under SD conditions compared to wild type (WT) (McNellis et al. 1994; Laubinger et al. 2006). In LD, the COP1-SPA complex is inhibited during the day period by cryptochrome 2 (cry2), which is required for early flowering under these conditions (Guo et al. 1998; Zuo et al. 2011). COP1 is also a well-known molecular player directly interacting with the UV-B photoreceptor UV RESISTANCE LOCUS 8 (UVR8) (Favory et al. 2009; Rizzini et al. 2011; Cloix et al. 2012; Yin et al. 2015; Jenkins 2017; Podolec and Ulm 2018). However, despite

this and the fact that UV-B is an intrinsic part of sunlight, our molecular understanding of photoperiodic flowering regulation in *Arabidopsis* is basically based on growth chamber experiments in the absence of UV-B. Thus, the role of UVR8 signaling in photoperiodic control of flowering time has not been previously investigated.

The seven-bladed β-propeller protein UVR8 forms homodimers in the absence of UV-B (Favory et al. 2009; Rizzini et al. 2011). UVR8 monomerizes upon UV-B absorption by specific intrinsic tryptophan residues, which is followed by interaction with COP1 (Favory et al. 2009; Rizzini et al. 2011). As a result of this UV-B-dependent interaction, the COP1 target protein ELONGATED HYPOCOTYL 5 (HY5) is stabilized (Favory et al. 2009; Huang et al. 2013; Binkert et al. 2014). HY5 is a bZIP transcription factor that plays a central role in light signaling (Lau and Deng 2012), including UVR8-mediated UV-B signaling (Ulm et al. 2004; Brown et al. 2005; Stracke et al. 2010; Binkert et al. 2014). The UVR8 photocycle involves negative feedback regulation by REPRESSOR OF UV-B PHOTOMORPHOGENESIS 1 (RUP1) and RUP2, which are UVR8-interacting proteins that facilitate the ground state reversion of UVR8 via redimerization (Gruber et al. 2010; Heijde and Ulm 2013). RUP1 and RUP2 act largely redundantly for all UV-B responses characterized to date and their role is to establish UVR8 homodimer/monomer equilibrium under diurnal conditions (Gruber et al. 2010; Heijde and Ulm 2013; Findlay and Jenkins 2016). A recent report has suggested that an apparently UV-B-independent role of RUP1 and RUP2 in flowering time regulation exists (note that EARLY FLOWERING BY OVEREXPRESSION 1/EFO1 = RUP1 and EFO2 = RUP2) (Wang et al. 2011). However, the underlying molecular mechanism and the role of RUP1 and RUP2 in photoperiodic flowering regulation have remained enigmatic. Here we report how RUP2 functions as a key repressor of UVR8-mediated induction of flowering through regulation of CO

activity, and that this function is crucial to distinguish non-inductive SD from inductive LD, thus enabling photoperiodic flowering.

Results

RUP2 is a repressor of flowering under short-day conditions containing UV-B

Flowering time regulation in natural ecological settings is complex and often distinct from that under laboratory conditions (Weinig et al. 2002; Wilczek et al. 2009; Brachi et al. 2010). UV-B is an important part of the sunlight spectrum that is usually lacking in controlled growth chamber environments. To better understand the potential roles of UV-B and RUP1/RUP2 in the regulation of flowering, we grew WT, *rup1*, *rup2*, and *rup1 rup2* plants under LD (16h/8h light/dark) and SD conditions (8h/16h light/dark). In contrast to a previous report (Wang et al. 2011), the flowering time and leaf number at flowering for *rup2* as well as *rup1 rup2* was comparable to that in WT under standard laboratory growth conditions, i.e. in the absence of UV-B (LD-UV and SD-UV) (Fig. 1A–C). Strikingly, however, *rup2* as well as *rup1 rup2* flowered much earlier than WT in SD in the presence of UV-B (SD+UV) (Fig. 1A–C). This early-flowering phenotype was specific to *rup2*, as *rup1* flowered similarly as WT (Fig. 1A–C). Moreover, the early-flowering phenotype of *rup2* and *rup1 rup2* in SD+UV was indistinguishable and, importantly, dependent on the UV-B photoreceptor UVR8, as *rup2 uvr8* and *rup1 rup2 uvr8* plants flowered as late as WT and *uvr8* (Fig. 1D,E and Fig. S1). Of note, the striking early-flowering phenotype of *rup2* under SD+UV was rescued by transgenic expression of the genomic *RUP2* locus with an approximate 1.5 kb promoter region (*rup2-1*/*Pro$_{RUP2}$:RUP2*) and was also observed in *rup2-2* plants carrying a different T-DNA insertion in *RUP2* than *rup2-1* (Fig. S2). Under LD conditions, the flowering phenotype of *rup1*, *rup2*, and *rup1 rup2* was not

different to that of WT, both in the absence and presence of UV-B (Fig. 1B,C). In fact, *rup2* plants under SD+UV flowered with as few leaves as WT and *rup2* under LD conditions (Fig. 1B), indicating that *RUP2* mutation rendered *Arabidopsis* from a facultative long-day to a day-neutral plant. We conclude that RUP2 is essential to inhibit flowering under non-inductive SD conditions, specifically in the presence of UV-B perceived by the UVR8 photoreceptor.

We further tested whether RUP2-overexpression represses flowering under LD conditions. However, RUP2 overexpression plants flowered as early as WT plants both in LD-UV and LD+UV (Fig. S3A,B), despite strongly elevated RUP2 levels (Fig. S3C). It should be noted that RUP2 overexpression is associated with a strong UV-B hyposensitive phenotype, resembling the "UV-B blindness" of *uvr8* null mutants (Gruber et al. 2010). We thus conclude that RUP2 overexpression cannot repress flowering under LD conditions. However, blocking UVR8 activation precludes analysis of a distinct effect of RUP2 overexpression on the UVR8-induced flowering pathway. Moreover, in contrast to the results in a previous publication (Wang et al. 2011), we did not observe an early-flowering phenotype for the RUP2 overexpression line in SD (Fig. S3D,E).

It has been previously shown that UVR8 overexpression lines display a similarly enhanced UV-B phenotype at the seedling stage as *rup2* and *rup1 rup2* (Favory et al. 2009; Gruber et al. 2010). To test whether over-activation of the UV-B signaling pathway leads to early flowering under SD+UV, we used an established UVR8-overexpression line (Favory et al. 2009). As expected, the UVR8-overexpression line displayed a similar morphology in response to UV-B exposure compared to that of *rup2*, such as smaller rosettes (Fig. S4A). However, UVR8 overexpression did not affect the flowering time in comparison to that in WT (Fig. S4B,C). It is of note that UVR8 overexpression was associated with strongly enhanced RUP2 levels (Fig.

S4D). Our data suggest that over-activation of the UVR8 signaling pathway is not sufficient to induce early flowering, likely due to the balancing effect of elevated RUP2 activity as a repressor of flowering.

We further tested the importance of RUP2 repression of early flowering in SD+UV in sun simulators that allow growth under a natural spectral balance from ultraviolet to infrared (Thiel et al. 1996). Under these more realistic irradiation conditions, *rup2* plants maintained an early-flowering phenotype, which contrasted with that of WT, *rup1*, *uvr8*, and *rup2 uvr8* plants (Fig. 2), thus confirming and further strengthening the results generated using plants grown in growth chambers containing UV-B. Therefore, we conclude that a major role of RUP2 concerns the repression of UVR8-induced flowering in SD+UV, which is an activity crucial for photoperiodic flowering under natural irradiation conditions, including UV-B.

RUP2 interacts with CO

To better understand the role of RUP2 as a repressor of flowering, we performed a yeast two-hybrid screen, which identified the B-box proteins CONSTANS-LIKE 1 (COL1)/BBX2, COL2/BBX3, and COL5/BBX6 as RUP2-interacting partners (Fig. S5). As *rup2* shows an early-flowering phenotype (Fig. 1) and the COL family members are highly related to the eponymous key flowering time regulator CO/BBX1 (Putterill et al. 1995; Khanna et al. 2009), we assessed the direct interaction between RUP2 and CO in yeast. Indeed, yeast two-hybrid growth assays indicated that RUP2 interacts with full length CO (Fig. 3A). In contrast to the CO-COP1 interaction (Liu et al. 2008; Fig. 3A), the N-terminal 183 amino acids of CO are sufficient for the interaction with RUP2, whereas the C-terminal CCT domain of CO is not required for interaction with RUP2 (Fig. 3A).

CO was found to be highly unstable in protein extracts, which precluded co-immunoprecipitation experiments. We thus resorted to Förster resonance energy transfer - fluorescence lifetime imaging microscopy (FRET-FLIM) as a cell biological assay for protein-protein association in transiently transformed *Nicotiana benthamiana* epidermal leaf cells. First, we observed that RUP1-GFP and RUP2-GFP localized to the nucleus in a diffuse manner when expressed alone or together with an NLS-mCherry, but aggregated in nuclear speckles when co-expressed with CO-mCherry (Fig. 3B). Further supporting CO-RUP interaction in yeast, our *in planta* FRET-FLIM analysis detected highly significant changes in the lifetime of the donor RUP1-GFP and RUP2-GFP fusions in the nucleus when co-expressed with CO-mCherry (Fig. 3C). In contrast, we did not observe significant GFP fluorophore lifetime changes when RUP1-GFP and RUP2-GFP were expressed alone or with NLS-mCherry (Fig. 3C). We thus conclude that RUP1 and RUP2 are closely associated with the key flowering regulator CO in plant cells.

Early flowering of rup2 in SD+UV depends on the flowering time regulator CO and its target FT

Our finding that RUP2 interacts with CO suggests that *rup2* early flowering may depend on CO activity. Indeed, the early-flowering phenotype of *rup2* in SD+UV was completely suppressed in *rup2 co* double mutants (Fig. 4). CO is an activator of *FT* expression that encodes the florigen FT, a major positive regulator of flowering time (Turck et al. 2008). In agreement with the *rup2* early-flowering phenotype under SD+UV, *FT* expression was indeed upregulated in *rup2* and *rup1 rup2* compared to that in WT, *rup1*, and *rup1 rup2 uvr8* plants (Fig. 5A). Furthermore, *FT* promoter-driven GUS expression (*Pro$_{FT}$:GUS*) in the leaf vasculature under SD+UV was enhanced in the *rup2* background in comparison to that in WT, *uvr8*, and *rup2 uvr8* backgrounds (Fig. 5B). Our findings suggest that *rup2* early flowering depends on enhanced CO-regulated *FT*

182 expression and thus FT activity. Indeed, the early-flowering phenotype of *rup2* under SD+UV
183 was completely suppressed in *rup2 ft* double mutants (Fig. 5C–E). We thus conclude that *FT*
184 expression is deregulated in *rup2* due to enhanced CO activity, and that active FT is required for
185 early flowering of *rup2* under SD+UV.
186
187 *RUP2 represses CO binding to the FT promoter*
188 Our findings that mutation of RUP2 affects flowering in a CO-dependent manner and that RUP2
189 interacts with CO suggest that RUP2 may regulate CO post-transcriptionally. In agreement, the
190 expression pattern of *CO* was not altered in *rup2* compared to that in WT during a 24h time
191 course under SD+UV conditions, excluding any effect on the diurnal regulation of *CO* mRNA
192 levels (Fig. 6A,B). As endogenous CO levels have never been detected in WT, we expressed a
193 *Pro$_{35S}$:3HA-CO* transgene in *rup2* plants. As described before (Song et al. 2012), HA-tagged CO
194 was detectable on protein immunoblots and its expression in a WT background resulted in
195 accelerated flowering in SD (Fig. 6C–E). This effect was also detectable in the *rup2* mutant
196 background, thus strongly diminishing the effect of *RUP2* mutation on flowering time under
197 SD+UV (Fig. 6C,D). Although this caveat has to be taken into consideration, regulation of
198 diurnal protein dynamics of overexpressed HA-CO was not affected by *RUP2* loss-of-function
199 when compared to WT (Fig. 6E). We further tested whether RUP2 has an effect on CO activity.
200 Indeed, chromatin immunoprecipitation (ChIP) assays of HA-CO showed strongly enhanced
201 binding to the *FT* promoter in *rup2* compared to that in the WT background in plants grown
202 under UV-B (Fig. 6F). In agreement with enhanced CO activity and thus *FT* expression, transient
203 transcription-activity assays revealed enhanced *FT*-promoter activation by CO in protoplasts
204 deficient of RUP2 compared to those with wild-type RUP2 (Fig. 6G). We thus conclude that

RUP2 represses CO activity on *FT* expression by interfering with its *FT* promoter-binding capacity.

Discussion

Seasonal patterns of flowering are of great importance for the reproductive success of many plants in natural ecosystems, as well as in horticulture and agricultural production systems. The impact of day length on flowering has been studied since the discovery of photoperiodism in 1920 (Garner and Allard 1920). In recent decades, the genetic pathways and regulatory proteins that promote flowering in response to photoperiod were largely defined in the model species *Arabidopsis thaliana* (Turck et al. 2008; Andres and Coupland 2012; Song et al. 2015). However, most of the work was and still is performed in growth chambers whose light spectrum does not include UV-B, an intrinsic portion of sunlight. Here, using controlled growth environments containing UV-B, we identified and characterized the unanticipated role of RUP2 in photoperiodic flowering control as a crucial repressor of CO activity associated with UVR8-inducible flowering in SD. RUP2-mediated prevention of flowering thus contributes to the perception of day length by allowing discrimination of SD from LD in the presence of UV-B.

CO is a B-box family transcriptional regulator that is a key activator of flowering by inducing *FT* expression. Thus, the activity of CO is regulated at many levels, including transcription, phosphorylation status, protein stability, and activity (Romera-Branchat et al. 2014; Song et al. 2015; Shim et al. 2017). Under inductive LD conditions, CO accumulates toward the end of the day, forming a complex with the histone-fold domain containing dimeric B and C subunits of Nuclear Factor Y (NF-Y) (Ben-Naim et al. 2006; Wenkel et al. 2006; Jang et al. 2008; Gnesutta et al. 2017). The CCT domain of CO within the heterotrimeric NF-CO complex

conveys binding specificity to the CO-responsive elements (*CORE*) in the *FT* promoter, thereby promoting *FT* expression near dusk (Gnesutta et al. 2017). Here, we provide evidence that RUP2 is a major repressor of CO activity under non-inductive SD+UV conditions, since *rup2* plants flower very early under SD+UV conditions. Moreover, as this early-flowering phenotype is suppressed in *rup2 uvr8* and *rup2 co* double mutants, it is thus UVR8- and CO-dependent. RUP2 apparently does not affect *CO* transcription or CO protein levels, but its repressive activity involves direct interaction with CO. Indeed, CO transcriptional activity is repressed by RUP2, and this effect is detectable at the level of reduced *FT* expression, *FT* promoter activity in transient reporter assays, and CO association with the *FT* promoter in ChIP assays. Interestingly, several CO-interacting proteins were recently described as negative regulators of CO transcriptional activity, acting through recruitment of TOPLESS repressor proteins or through inhibition of CO binding to target genes (Wang et al. 2014; Nguyen et al. 2015; Zhang et al. 2015; Graeff et al. 2016; Wang et al. 2016; Xu et al. 2016; Ordonez-Herrera et al. 2018), the latter of which is similar to our findings for RUP2 activity. It is interesting to note that RUP2 binds to the N-terminal part of CO, which is comprised of two tandem B-box domains. This interaction could directly affect binding of CO to target promoters. Alternately, this interaction may facilitate the binding of a presently unknown repressor of CO and/or may prevent interaction with a positive-regulatory interaction partner by blocking the interaction site.

If RUP2 was a general repressor of CO activity in the absence of UV-B, we would expect delayed flowering in RUP2 overexpression lines particularly under LD-UV conditions and early flowering in *rup2* plants in SD-UV. Previous work has suggested that overexpression of *RUP2*/*EFO2* results in early flowering in both SD and LD (Wang et al. 2011); a phenotype that we, however, did not observe in our experimental conditions using lines for which RUP2

overexpression was clearly confirmed by immunoblot analysis. Furthermore, we did not observe delayed flowering of RUP2-overexpression lines in LD-UV or early flowering of *rup2* in SD-UV. This suggests that RUP2 affects photoperiodic flowering very specifically for a distinct UVR8-induced CO activation mechanism. As CO-FT regulation is largely localized to phloem companion cells in the leaf vasculature (Takada and Goto 2003; Turck et al. 2008; Song et al. 2015), the tissue-specificity of UVR8 and RUP2 activity in the regulation of flowering remains to be determined, as well as the exact mechanism by which UVR8 activates CO.

Interpretation of the lack of a RUP2 overexpression effect in LD+UV is complicated due to the fact that UVR8 activity is fully repressed by RUP2 overexpression (Gruber et al. 2010; Heijde and Ulm 2013). Indeed, RUP2-overexpression lines mimic the phenotype of *uvr8* null mutants, and indeed, no UVR8 monomers and no physiological response was detected in these lines upon UV-B treatment (Gruber et al. 2010; Heijde and Ulm 2013). It is thus clear that UVR8-mediated activation of flowering is impaired at the level of photoreceptor regulation in RUP2 overexpression lines, and an independent effect on CO activity cannot be investigated as no UVR8-mediated signaling occurs with RUP2 overexpression. Notwithstanding this, it is of note that the role of RUP2 in flowering time regulation seems independent of its role in the regulation of UVR8 activity. This is particularly highlighted by the fact that UVR8 overexpression plants do not show early flowering although they display a similar UV-B hypersensitivity as in *rup2* as determined by the rosette phenotype. This is further supported by the interaction of RUP2 with CO and its effect on CO transcriptional activity and *FT* promoter binding.

It is noteworthy that WT develops slower and flowers later under SD+UV than under SD-UV conditions (e.g. Figs. 1, 4A–C, and 5C–E), which is in agreement with a recent report (Dotto

et al. 2018). Interestingly, this delayed flowering is partially UVR8-dependent (Figs. 1D,E, and S1) and has previously been linked to the age pathway of flowering (Dotto et al. 2018). The potential interplay between the effects of UVR8 signaling on the age and photoperiod pathway remains to be determined; however, it is clear that the effect of RUP2 mutation on the photoperiodic pathway overrides the potential effect of UVR8-hyperactivity in *rup2* on the age pathway. Moreover, it is of note that the delay in flowering under UV-B is not detectable in the sun simulator experiment, but the repressor function of RUP2 clearly is (Fig. 2).

Seasonal responses of flowering time assessed in field trials are not always as anticipated based on experiments performed under laboratory conditions (Weinig et al. 2002; Wilczek et al. 2009; Brachi et al. 2010; Andres and Coupland 2012). In part, the absence of UV-B in most laboratory experiments may contribute to this phenomenon; however, such a notion needs to be experimentally further verified. Independent of this, we show that RUP2 loss-of-function renders the facultative long-day species *Arabidopsis thaliana* into a day-neutral plant in the presence of UV-B, demonstrating that RUP2 is required for flowering time regulation by day length under natural conditions. It remains to be investigated whether RUP2 may integrate other environmental factors to regulate flowering in the field, under sunlight with its intrinsic UV-B. For example, it can be envisaged that RUP2 degradation may be a potent inducer of flowering in non-inductive photoperiods, a possibility that deserves further investigation.

Material and Methods

Plant material and growth conditions

The mutants and overexpression lines used in this study were in the *Arabidopsis thaliana* Columbia (Col) accession and were described previously as follows: *uvr8-6* (Favory et al. 2009),

297 *rup1-1*, *rup2-1*, *rup2-1*/*Pro$_{35S}$:RUP2* (Gruber et al. 2010), *cop1-4* (Deng et al. 1992), *ft-10* (Yoo
298 et al. 2005), *co-101* (Takada and Goto 2003), and *Pro$_{35S}$:3HA-CO* line #7 (Song et al. 2012).
299 *rup2-2* (SALK_139836) (Alonso et al. 2003) was characterized in this study (Fig. S6). The GUS
300 reporter lines used were *Pro$_{FT}$:GUS* (Takada and Goto 2003), which was introgressed into *rup2-*
301 *1*, *uvr8-6*, and *rup2-1 uvr8-6* mutants by genetic crossing, and *gCO:GUS* (Takada and Goto
302 2003), which was introgressed into *rup2-1*. The *RUP2* (At5g23730) genomic locus including
303 approximately 1.5 kb promoter region was amplified with primers RUP2pFW (5′- GGG G*AC*
304 *AAG TTT GTA CAA AAA AGC AGG CT*T CCA CGT ATG ACT CGT CCT TAC TTT GC -3′;
305 *att*B1 site italic, gene specific sequence underlined) and RUP2pREV (5′- GGG G*AC CAC TTT*
306 *GTA CAA GAA AGC TGG GT*C ATG AAA ACA GAG TAA TGA CTG TTG C -3′; *att*B2 italic,
307 gene specific sequence underlined), cloned into pDONR207 using Gateway technology
308 (Invitrogen) and sequenced to confirm integrity of the cloned fragment. The genomic clone was
309 inserted into the binary destination vector pMDC163 (Curtis and Grossniklaus 2003). *rup2-1*
310 plants were transformed by Agrobacterium using the floral dip method (Clough and Bent 1998).
311 For flowering time experiments, qRT-PCR, GUS reporter assays, and transient expression
312 assays, seeds were stratified for 2 days at 4°C in the dark and plants were grown with a day/night
313 temperature cycle of 22°C/18°C in GroBanks (CLF Plant Climatics) with Philips Master TL-D
314 58W/840 white-light fluorescent tubes (120 μmol m^{-2} s^{-1}; measured with a LI-250 Light Meter;
315 LI-COR Biosciences), supplemented or not with UV-B from Philips TL40W/01RS narrowband
316 UV-B tubes (0.07 mW cm^{-2}; measured with a VLX-3W Ultraviolet Light Meter equipped with a
317 CX-312 sensor; Vilber Lourmat). Plants were grown under 8h/16h light/dark SD or 16h/8h
318 light/dark LD conditions, as indicated.

For immunoblot analysis, ChIP, hypocotyl length measurement and anthocyanin quantification, seeds were surface-sterilized with 70% ethanol and 0,005% Tween 20, plated on half-strength MS medium (Duchefa) containing 1% sucrose and 0.8% agar. For hypocotyl length measurement and anthocyanin quantification seedlings were grown as described previously (Oravecz et al. 2006; Favory et al. 2009). For immunoblot analysis, qRT-PCR, and ChIP, seedlings were grown in GroBanks under SD-UV or SD+UV conditions, as indicated.

A sun simulator of the Research Unit Environmental Simulation at the Helmhotz Zentrum München (Thiel et al. 1996) was used to study flowering time regulation under conditions simulating natural light and UV-radiation conditions. The condition of the treatment in the sun simulator was similar as described previously (Favory et al. 2009; Gruber et al. 2010; González Besteiro et al. 2011) with a 8-h day period with mean photosynthetically active radiation (PAR; 400–700 nm) of 600 μmol m^{-2} s^{-1} and 6 h of UV-B irradiance with a biologically effective radiation of 308 mW m^{-2} (weighted by the generalized plant action spectrum (Caldwell 1971), normalized at 300 nm; Fig. S7). Controls were grown excluding the entire UV radiation spectrum. The temperature was maintained at 23°C during the day and 18°C at night. The relative humidity was kept constant at 60%.

PCR genotyping of mutants and isolation of double mutants

Single mutants were crossed and the double mutants identified by PCR genotyping in the F2 generation. *rup1-1*, *rup2-1*, and *uvr8-6* were genotyped as previously described (Gruber et al. 2010). *co-101*, *ft-10*, and *rup2-2* were genotyped as follows:

co-101: CO101_LP (5′-AGC TCC CAC ACC ATC AAA CTT ACT ACA TC-3′) + CO101_RP (5′-AGT CCA TAC TCG AGT TGT AAT CCA-3′) = 0.6 kb for WT; CO101_LP +

T-DNA primer LB3 (5′-TAG CAT CTG AAT TTC ATA ACC AAT CTC GAT ACA C-3′) = 0.45 kb for *co-101*.

ft-10 (GABI_290E08): FT10_LP (5′-ATA TTG ATG AAT CTC TGT TGT GG-3′) + FT10_RP (5′-AGG GTT GCT AGG ACT TGG AAC A-3′) = 0.3 kb for WT; T-DNA primer 8474 (5′-ATA ATA ACG CTG CGG ACA TCT ACA TTT T-3′) + FT_RP = 0.5 kb for *ft-10*.

rup2-2 (SALK_139836): RUP2_SALK_139836_LP (5′-TGT TTC GGT GTT ACC ATT ACG-3′) + RUP2_SALK_139836_RP (5′-TCG GAT CCC ATA CTT GCA TAG-3′) = 1.0 kb for WT; T-DNA primer LBb1.3 (5′-ATT TTG CCG ATT TCG GAA C-3′) + RUP2_SALK_139836_RP = 0.5 kb for *rup2-2*.

Immunoblot analysis

Proteins were extracted in 50 mM Na-phosphate (pH 7.4), 150 mM NaCl, 10% glycerol, 5 mM EDTA, 1 mM DTT, 0.1% Triton X-100, 50 μM MG132, 2mM Na_3VO_4, 2 mM NaF, and 1% (vol/vol) protease inhibitor mixture for plant extracts (P9599; Sigma-Aldrich). For immunoblot analysis, total cellular proteins were separated by electrophoresis in 10% (wt/vol) SDS polyacrylamide gels and transferred to PVDF membranes according to the manufacturer's instructions (iBlot Dry Blotting System, Thermo Fisher Scientific).

Rabbit polyclonal antibodies were generated against synthetic peptides derived from the RUP2 protein sequence (amino acids 1-15 + C: MNTLHPHKQQQEQAQC; anti-$RUP2^{(1-15)}$) and were affinity-purified against the peptide (Eurogentec). Anti-$RUP2^{(1-15)}$, anti-$UVR8^{(426-440)}$ (Favory et al. 2009), anti-HA.11 (901513; BioLegend) and anti-actin (A0480, Sigma-Aldrich) were used as primary antibodies. Horseradish peroxidase (HRP)-conjugated anti-rabbit and anti-mouse immunoglobulins (Dako A/S) were used as the secondary antibodies. Chemiluminescent

signals were generated with the ECL Plus Western Detection Kit and revealed with an ImageQuant LAS 4000 mini CCD camera system (GE Healthcare).

Yeast two-hybrid interaction assays

A yeast two-hybrid screen was performed using RUP2 as bait fused to the GAL4 binding domain (Matchmaker Gold Yeast Two-Hybrid System, Clontech). The screen was carried out following the standard protocol suggested by the manufacturer.

Arabidopsis RUP1 (At5g52250) and *RUP2* coding sequences were cloned into yeast two-hybrid plasmid containing a DNA binding domain (pGBKT7-GW) (Yin et al. 2015) and *CO* into plasmid containing an activation domain (pGADT7-GW). Bait and prey constructs were transformed into *S. cerevisiae* strain Y2H Gold and Y187, respectively. To quantify protein-protein interaction using CPRG as a substrate yeast growth was carried out directly on plate as described before (Rizzini et al. 2011), and the assay was performed according to the protocol described in Yeast Protocols Handbook (Clontech, Version PR973283). The lacZ β-galactosidase activity is expressed as Miller units.

Anthocyanin extraction and measurement

Arabidopsis seedlings were grown for 4 days under low narrowband UV-B fields with the appropriated cut-off filters, as previously described (Oravecz et al. 2006; Favory et al. 2009). Fifty-mg of seedlings were harvested from agar plates and immediately frozen in liquid nitrogen. Sample tissues were processed for 10 seconds using a Silamat S5 mixer (Ivoclar Vivadent). 250µl of acidic methanol (1% HCl, [w/v]) was added to each sample that was homogenised and placed in an overhead shaker at 4°C for 1 hour as described before (Yin et al. 2012). Samples

were centrifuged for 1 minute at 14,000 rpm and the supernatant was used to quantify anthocyanin content in a spectrophotometer at 535nm and 650nm. Values were reported as A530 − 0.25 (A657) g^{-1} fresh weight.

Hypocotyl length

Four-d-old *Arabidopsis* seedlings were grown in the appropriated light conditions and their hypocotyl lengths were measured (n > 30) using ImageJ software as described previously (Oravecz et al. 2006).

Statistical analysis of flowering time experiments

ANOVA with post-hoc Tukey HSD statistical analyses were performed using the R software package. The means and SD are derived from replicated independent biological samples, unless otherwise stated. Shared letters indicate no statistically significant difference in the means (P > 0.05).

CLSM and FLIM analyses

For CLSM and FLIM analysis, the binary 2in1 Vectors were used (Hecker et al. 2015). The coding sequences of *RUP1* or *RUP2* were cloned into the donor plasmid (mEGFP) while *UVR8* or *CO* were cloned into acceptor plasmid (mCherry) using the MultiSite Gateway Technology (Invitrogen). mCherry fused to an NLS was used as a negative control. These constructs were transformed into *Agrobacterium tumefaciens* strain GV3101 and infiltrated into *Nicotiana benthamiana* leaves as described previously (Hecker et al. 2015). Leaves were subjected to CLSM and FLIM analyzed 1–2 days post infiltration.

411 The measurements were performed as described previously (Hecker et al. 2015). Briefly,
412 all CLSM and FLIM measurements were performed using a Leica TCS SP8 confocal microscope
413 (Leica Microsystems) equipped with a FLIM unit (PicoQuant). Images were acquired using a
414 63x/1.20 water immersion objective. For the excitation and emission of fluorescent proteins
415 following settings were used: mEGFP at excitation 488 nm and emission 495–530 nm; mCherry
416 at excitation 561 nm and emission 580–630 nm.
417 FLIM data derived from measurements of at least 20 nuclei for each fusion protein
418 combination. To excite RUP1-mEGFP and RUP2-mEGFP for FLIM experiments, a 470 nm
419 pulsed laser (LDH-P-C-470) was used, and the corresponding emission was detected with a
420 SMD Emission SPFLIM PMT 495–545 nm by time-correlated single-photon counting using a
421 Picoharp 300 module (PicoQuant). Each time-correlated single-photon counting histogram was
422 reconvoluted with the corresponding instrument response function and fitted against a
423 monoexponential decay function for donor-only samples and a biexponential decay function for
424 the other samples to unravel the mEGFP fluorescence lifetime of each nucleus.
425 The average mEGFP fluorescence lifetimes as well as the standard error values were
426 calculated using Microsoft Excel 2013. Statistical analysis was performed with JMP (version
427 12.2.0). To test for homogeneity of variance, Levene's test ($df=5/140$, $F=26.298$, $P < 0.0001$)
428 was used and statistical significance was calculated by a two-tailed, all-pair Kruskal-Wallis test
429 followed by a Steel-Dwass post hoc correction.
430
431 *GUS staining*
432 *Arabidopsis* leaves were fixed in 90% acetone for 30 min. After washing three times in ice-cold
433 water, plant tissues were incubated with staining buffer [0.5 mg/ml 5-bromo-4-chromo-3-

indolyl-β-d-glucuronide (X-Glc), 10 mm EDTA, 0.5 mm ferricyanide, 0.5 mm ferrocyanide, and 0.1% Triton X-100 in phosphate buffer] for 5 min at 4°C followed by incubation at 37°C. After removal of staining solution, tissue was cleared by successive washes with 75% ethanol. Samples were mounted in glycerol and analyzed using a stereomicroscope (Leica MZ16, Leica Microsystems AG, Heerbrugg, Switzerland) or a differential interference contrast (DIC) microscope (Zeiss Axioscope II, Carl Zeiss AG, Feldbach, Switzerland, or Nikon Eclipse 80i, Nikon AG, Egg, Switzerland).

Quantitative real-time PCR

Arabidopsis total RNA was isolated with the Plant RNeasy kit according to the manufacturer's instructions (Qiagen), followed by DNaseI treatment. In order to inactivate DNAse I, 20 mM EDTA was added and samples were incubated at 65°C for 10 minutes. Synthesis of the first strand of cDNA was performed using the TaqMan Reverse Transcription Reagents kit according to the manufacturer's standard protocol (Thermo Fisher Scientific). Each qRT-PCR reaction was composed by cDNA synthesized with a 1:1 mixture of oligo(dT) primers and random hexamers from 25 ng of total RNA. PCR reactions were performed using the ABsolute QPCR Rox Mix Kit (ABgene) and a QuantStudio 5 Real-Time PCR system (Thermo Fisher Scientific). The following primers were used: for *CO* (At5g15840), CO_qRT_fw (5′-CCT CAG GGA CTC ACT ACA ACG-3′) and CO_qRT_rv (5′-TCT TGG GTG TGA AGC TGT TG-3′), and for *FT* (At1g65480), FT_qRT_fw (5′-CCA AGA GTT GAG ATT GGT GGA-3′) and FT_qRT_rv (5′-ATT GCC AAA GGT TGT TCC AG-3′). The level of expression of 18S and *UBQ10* (Czechowski et al. 2005) were used to normalize the concentrations of the various mRNA samples in which gene expression was analysed using qbasePLUS real-time PCR data analysis

software version 2.4 (Biogazelle). Each reaction was performed in technical triplicates; data shown are representative of at least two biological repetitions.

ChIP

Samples were cross-linked in 3% formaldehyde solution in PBS and cross-linking was quenched with 0.2M glycine. Nuclei enrichment was performed as described (Fiil et al. 2008). Samples were sonicated in lysis buffer (50mM Tris-HCL, pH8; 10mM EDTA; 1% SDS) and further processed as described (Stracke et al. 2010; Binkert et al. 2014). The chromatin was immunoprecipitated with anti-HA antibody (ChIP grade, Abcam; ab9110) overnight at 4°C, after which crosslinking was reversed for 2 h at 85°C. DNA was purified using QIAquick PCR Purification Kit (Qiagen) before analysis with a QuantStudio 5 Real-Time PCR system (Thermo Fisher Scientific) and the following primer sets: Pro_{FT_-100}-Fw (5′-AGA GGG TTC ATG CCT ATG ATA C-3′) and Pro_{FT_-100}-Rv (5′-CTT TGA TCT TGA ACA AAC AGG TG-3′) (Bu et al. 2014); and Pro_{FT_-1185}-Fw (5′-TTA TCC TGG TCG TGC AAA TG-3′) and Pro_{FT_-1185}-Rv (5′-CAA GCG GCC ATA TTA TGG AA-3′) (Song et al. 2012). qPCR data were analyzed according to the percentage of input method (Haring et al. 2007).

Transient expression assays in protoplasts

For the Pro_{FT}*:fLUC* reporter construct, *FT* promoter region (-1 to -5722) was amplified with primers oVCG-475 (5′-CCC CC*C TCG AG*G TCG ACA TTT GCT GAA CAA AAA TCT ATT-3′; XhoI site italic, gene specific sequence underlined) and oVCG-476 (5′-GGT G*GC GGC CGC* TCT AGC TTT GAT CTT GAA CAA ACA GGT G-3′; NotI site italic, gene specific sequence

underlined) from the BAC clone F5I14 and cloned into pGREENII 0800-LUC XhoI/NotI restriction sites (Hellens et al. 2005).

Protoplasts were isolated from 4–8-week-old *co-101* and *rup2-1 co-101* plants growing under SD+UV. Expanded leaves were harvested and protoplast was prepared as previously described (Wu et al. 2009). Each protoplast transfection was performed with 5 µg of Pro_{FT}*:fLUC* and Pro_{35S}*:CO* plasmids and incubated overnight in darkness at 21°C. Luciferase assay was performed with Dual-Luciferase Reporter Assay System (Promega) at Zeitgeber time (ZT; ZT0 = lights on, ZT8 = lights off) 3–4 following manufacturer's instructions and a GloMax 96 Microplate Luminometer (Promega). Relative luciferase activity corresponds to normalized firefly/renilla ratio.

Acknowledgments

We thank Takato Imaizumi and Koji Goto for providing plant material, Christopher Grefen for the binary 2in1 vectors, Hongtao Liu for the pGREENII 0800-LUC construct, Rodrigo S. Reis for technical assistance with protoplast transient expression assays, Isabelle Fleury for contributing some of the crosses, Stefanie Mühlhans for excellent technical assistance in sun simulator experiments, and Michael Hothorn for helpful comments on the manuscript. This work was supported by the University of Geneva, the Swiss National Science Foundation (grant no. 31003A_175774 to R.U. and CRSII3_154438 to R.U. and C.F.), the European Research Council (ERC) under the European Union's Seventh Framework Programme (grant 310539 to R.U.), and the German Research Foundation (grant CRC 1101-D02 to K.H.). V.C.G. was supported by an EMBO long-term fellowship (ALTF 293-2013).

Author Contributions: A.B.A. and R.U. conceived and designed the study. A.B.A. performed all of the experiments reported here, except: N.G. and K.H. contributed the FRET-FLIM data (Fig. 3B,C), A.A. and J.B.W. contributed the sun simulator data (Figs. 2 and S7), M.P. contributed the chromatin immunoprecipitation data (Fig. 6F), S.C. contributed the protein immunoblots (Figs 6E, S3C, and S4D), V.C.G. and C.F. contributed the transient expression assays in protoplasts (Fig. 6G). R.U. supervised the research, and A.B.A. and R.U. wrote the manuscript, with input from all authors. The manuscript has been seen and approved by all authors.

References

Alonso JM, Stepanova AN, Leisse TJ, Kim CJ, Chen H, Shinn P, Stevenson DK, Zimmerman J, Barajas P, Cheuk R et al. 2003. Genome-wide insertional mutagenesis of *Arabidopsis thaliana*. *Science* **301**: 653-657.

Andres F, Coupland G. 2012. The genetic basis of flowering responses to seasonal cues. *Nat Rev Genet* **13**: 627-639.

Ben-Naim O, Eshed R, Parnis A, Teper-Bamnolker P, Shalit A, Coupland G, Samach A, Lifschitz E. 2006. The CCAAT binding factor can mediate interactions between CONSTANS-like proteins and DNA. *Plant J* **46**: 462-476.

Binkert M, Kozma-Bognar L, Terecskei K, De Veylder L, Nagy F, Ulm R. 2014. UV-B-responsive association of the Arabidopsis bZIP transcription factor ELONGATED HYPOCOTYL5 with target genes, including its own promoter. *Plant Cell* **26**: 4200-4213.

Brachi B, Faure N, Horton M, Flahauw E, Vazquez A, Nordborg M, Bergelson J, Cuguen J, Roux F. 2010. Linkage and association mapping of *Arabidopsis thaliana* flowering time in nature. *PLoS Genet* **6**: e1000940.

Brown BA, Cloix C, Jiang GH, Kaiserli E, Herzyk P, Kliebenstein DJ, Jenkins GI. 2005. A UV-B-specific signaling component orchestrates plant UV protection. *Proc Natl Acad Sci USA* **102**: 18225-18230.

Bu Z, Yu Y, Li Z, Liu Y, Jiang W, Huang Y, Dong AW. 2014. Regulation of Arabidopsis flowering by the histone mark readers MRG1/2 via interaction with CONSTANS to modulate *FT* expression. *PLoS Genet* **10**: e1004617.

Caldwell MM. 1971. Solar UV irradiation and the growth and development of higher plants. in *Photophysiology* (ed. AC Giese), pp. 131-177. Academic Press, New York.

Cloix C, Kaiserli E, Heilmann M, Baxter KJ, Brown BA, O'Hara A, Smith BO, Christie JM, Jenkins GI. 2012. C-terminal region of the UV-B photoreceptor UVR8 initiates signaling through interaction with the COP1 protein. *Proc Natl Acad Sci USA* **109**: 16366-16370.

Clough SJ, Bent AF. 1998. Floral dip: a simplified method for Agrobacterium-mediated transformation of *Arabidopsis thaliana*. *Plant J* **16**: 735-743.

Corbesier L, Vincent C, Jang S, Fornara F, Fan Q, Searle I, Giakountis A, Farrona S, Gissot L, Turnbull C et al. 2007. FT protein movement contributes to long-distance signaling in floral induction of Arabidopsis. *Science* **316**: 1030-1033.

Curtis MD, Grossniklaus U. 2003. A gateway cloning vector set for high-throughput functional analysis of genes in planta. *Plant Physiol* **133**: 462-469.

Czechowski T, Stitt M, Altmann T, Udvardi MK, Scheible WR. 2005. Genome-wide identification and testing of superior reference genes for transcript normalization in Arabidopsis. *Plant Physiol* **139**: 5-17.

Deng XW, Matsui M, Wei N, Wagner D, Chu AM, Feldmann KA, Quail PH. 1992. COP1, an Arabidopsis regulatory gene, encodes a protein with both a zinc-binding motif and a G beta homologous domain. *Cell* **71**: 791-801.

Dotto M, Gomez MS, Soto MS, Casati P. 2018. UV-B radiation delays flowering time through changes in the PRC2 complex activity and miR156 levels in *Arabidopsis thaliana*. *Plant Cell Environ* **41**: 1394-1406.

Favory JJ, Stec A, Gruber H, Rizzini L, Oravecz A, Funk M, Albert A, Cloix C, Jenkins GI, Oakeley EJ et al. 2009. Interaction of COP1 and UVR8 regulates UV-B-induced photomorphogenesis and stress acclimation in Arabidopsis. *EMBO J* **28**: 591-601.

Fiil BK, Qiu JL, Petersen K, Petersen M, Mundy J. 2008. Coimmunoprecipitation (co-IP) of nuclear proteins and chromatin immunoprecipitation (ChIP) from Arabidopsis. *CSH Protoc* **2008**: pdb prot5049.

Findlay KM, Jenkins GI. 2016. Regulation of UVR8 photoreceptor dimer/monomer photo-equilibrium in Arabidopsis plants grown under photoperiodic conditions. *Plant Cell Environ* **39**: 1706-1714.

Garner WW, Allard HA. 1920. Effect of the relative length of day and night and other factors of the environment on growth and reproduction in plants. *J Agric Res* **18**: 553–606.

Gnesutta N, Kumimoto RW, Swain S, Chiara M, Siriwardana C, Horner DS, Holt BF, 3rd, Mantovani R. 2017. CONSTANS imparts DNA sequence specificity to the histone fold NF-YB/NF-YC dimer. *Plant Cell* **29**: 1516-1532.

González Besteiro MA, Bartels S, Albert A, Ulm R. 2011. Arabidopsis MAP kinase phosphatase 1 and its target MAP kinases 3 and 6 antagonistically determine UV-B stress tolerance, independent of the UVR8 photoreceptor pathway. *Plant J* **68**: 727-737.

Graeff M, Straub D, Eguen T, Dolde U, Rodrigues V, Brandt R, Wenkel S. 2016. MicroProtein-mediated recruitment of CONSTANS into a TOPLESS trimeric complex represses flowering in Arabidopsis. *PLoS Genet* **12**: e1005959.

Gruber H, Heijde M, Heller W, Albert A, Seidlitz HK, Ulm R. 2010. Negative feedback regulation of UV-B-induced photomorphogenesis and stress acclimation in Arabidopsis. *Proc Natl Acad Sci USA* **107**: 20132-20137.

Guo H, Yang H, Mockler TC, Lin C. 1998. Regulation of flowering time by Arabidopsis photoreceptors. *Science* **279**: 1360-1363.

Haring M, Offermann S, Danker T, Horst I, Peterhansel C, Stam M. 2007. Chromatin immunoprecipitation: optimization, quantitative analysis and data normalization. *Plant Methods* **3**: 11.

Hecker A, Wallmeroth N, Peter S, Blatt MR, Harter K, Grefen C. 2015. Binary 2in1 vectors improve in planta (co)localization and dynamic protein interaction studies. *Plant Physiol* **168**: 776-787.

Heijde M, Ulm R. 2013. Reversion of the Arabidopsis UV-B photoreceptor UVR8 to the homodimeric ground state. *Proc Natl Acad Sci USA* **110**: 1113-1118.

Hellens RP, Allan AC, Friel EN, Bolitho K, Grafton K, Templeton MD, Karunairetnam S, Gleave AP, Laing WA. 2005. Transient expression vectors for functional genomics, quantification of promoter activity and RNA silencing in plants. *Plant Methods* **1**: 13.

Huang X, Ouyang X, Yang P, Lau OS, Chen L, Wei N, Deng XW. 2013. Conversion from CUL4-based COP1-SPA E3 apparatus to UVR8-COP1-SPA complexes underlies a distinct biochemical function of COP1 under UV-B. *Proc Natl Acad Sci USA* **110**: 16669-16674.

589 Jaeger KE, Wigge PA. 2007. FT protein acts as a long-range signal in Arabidopsis. *Curr Biol* **17**: 1050-1054.
590 Jang S, Marchal V, Panigrahi KC, Wenkel S, Soppe W, Deng XW, Valverde F, Coupland G. 2008.
591 Arabidopsis COP1 shapes the temporal pattern of CO accumulation conferring a photoperiodic
592 flowering response. *EMBO J* **27**: 1277-1288.
593 Jenkins GI. 2017. Photomorphogenic responses to ultraviolet-B light. *Plant Cell Environ* **40**: 2544-2557.
594 Khanna R, Kronmiller B, Maszle DR, Coupland G, Holm M, Mizuno T, Wu SH. 2009. The Arabidopsis B-box
595 zinc finger family. *Plant Cell* **21**: 3416-3420.
596 Lau OS, Deng XW. 2012. The photomorphogenic repressors COP1 and DET1: 20 years later. *Trends Plant*
597 *Sci* **17**: 584-593.
598 Laubinger S, Marchal V, Gentilhomme J, Wenkel S, Adrian J, Jang S, Kulajta C, Braun H, Coupland G,
599 Hoecker U. 2006. Arabidopsis SPA proteins regulate photoperiodic flowering and interact with
600 the floral inducer CONSTANS to regulate its stability. *Development* **133**: 3213-3222.
601 Liu LJ, Zhang YC, Li QH, Sang Y, Mao J, Lian HL, Wang L, Yang HQ. 2008. COP1-mediated ubiquitination of
602 CONSTANS is implicated in cryptochrome regulation of flowering in Arabidopsis. *Plant Cell* **20**:
603 292-306.
604 Mathieu J, Warthmann N, Kuttner F, Schmid M. 2007. Export of FT protein from phloem companion cells
605 is sufficient for floral induction in Arabidopsis. *Curr Biol* **17**: 1055-1060.
606 McNellis TW, von Arnim AG, Araki T, Komeda Y, Misera S, Deng XW. 1994. Genetic and molecular
607 analysis of an allelic series of *cop1* mutants suggests functional roles for the multiple protein
608 domains. *Plant Cell* **6**: 487-500.
609 Nguyen KT, Park J, Park E, Lee I, Choi G. 2015. The Arabidopsis RING domain protein BOI inhibits
610 flowering via CO-dependent and CO-independent mechanisms. *Mol Plant* **8**: 1725-1736.
611 Oravecz A, Baumann A, Mate Z, Brzezinska A, Molinier J, Oakeley EJ, Adam E, Schafer E, Nagy F, Ulm R.
612 2006. CONSTITUTIVELY PHOTOMORPHOGENIC1 is required for the UV-B response in
613 Arabidopsis. *Plant Cell* **18**: 1975-1990.
614 Ordonez-Herrera N, Trimborn L, Menje M, Henschel M, Robers L, Kaufholdt D, Hansch R, Adrian J, Ponnu
615 J, Hoecker U. 2018. The transcription factor COL12 is a substrate of the COP1/SPA E3 ligase and
616 regulates flowering time and plant architecture. *Plant Physiol* **176**: 1327-1340.
617 Podolec R, Ulm R. 2018. Photoreceptor-mediated regulation of the COP1/SPA E3 ubiquitin ligase. *Curr*
618 *Opin Plant Biol* **45**: 18-25.
619 Putterill J, Robson F, Lee K, Simon R, Coupland G. 1995. The CONSTANS gene of Arabidopsis promotes
620 flowering and encodes a protein showing similarities to zinc finger transcription factors. *Cell* **80**:
621 847-857.
622 Rizzini L, Favory JJ, Cloix C, Faggionato D, O'Hara A, Kaiserli E, Baumeister R, Schafer E, Nagy F, Jenkins GI
623 et al. 2011. Perception of UV-B by the Arabidopsis UVR8 protein. *Science* **332**: 103-106.
624 Romera-Branchat M, Andres F, Coupland G. 2014. Flowering responses to seasonal cues: what's new?
625 *Curr Opin Plant Biol* **21**: 120-127.
626 Samach A, Onouchi H, Gold SE, Ditta GS, Schwarz-Sommer Z, Yanofsky MF, Coupland G. 2000. Distinct
627 roles of CONSTANS target genes in reproductive development of Arabidopsis. *Science* **288**: 1613-
628 1616.
629 Shim JS, Kubota A, Imaizumi T. 2017. Circadian clock and photoperiodic flowering in Arabidopsis:
630 CONSTANS is a hub for signal integration. *Plant Physiol* **173**: 5-15.
631 Song YH, Shim JS, Kinmonth-Schultz HA, Imaizumi T. 2015. Photoperiodic flowering: time measurement
632 mechanisms in leaves. *Annu Rev Plant Biol* **66**: 441-464.
633 Song YH, Smith RW, To BJ, Millar AJ, Imaizumi T. 2012. FKF1 conveys timing information for CONSTANS
634 stabilization in photoperiodic flowering. *Science* **336**: 1045-1049.

635 Stracke R, Favory JJ, Gruber H, Bartelniewoehner L, Bartels S, Binkert M, Funk M, Weisshaar B, Ulm R.
636 2010. The Arabidopsis bZIP transcription factor HY5 regulates expression of the *PFG1*/*MYB12*
637 gene in response to light and ultraviolet-B radiation. *Plant Cell Environ* **33**: 88-103.
638 Takada S, Goto K. 2003. TERMINAL FLOWER2, an Arabidopsis homolog of HETEROCHROMATIN
639 PROTEIN1, counteracts the activation of *FLOWERING LOCUS T* by CONSTANS in the vascular
640 tissues of leaves to regulate flowering time. *Plant Cell* **15**: 2856-2865.
641 Thiel S, Döhring T, Köfferlein M, Kosak A, Martin P, Seidlitz HK. 1996. A phytotron for plant stress
642 research: how far can artificial lighting compare to natural sunlight? *J Plant Physiol* **148**: 456-
643 463.
644 Turck F, Fornara F, Coupland G. 2008. Regulation and identity of florigen: FLOWERING LOCUS T moves
645 center stage. *Annu Rev Plant Biol* **59**: 573-594.
646 Ulm R, Baumann A, Oravecz A, Mate Z, Adam E, Oakeley EJ, Schafer E, Nagy F. 2004. Genome-wide
647 analysis of gene expression reveals function of the bZIP transcription factor HY5 in the UV-B
648 response of Arabidopsis. *Proc Natl Acad Sci USA* **101**: 1397-1402.
649 Wang CQ, Guthrie C, Sarmast MK, Dehesh K. 2014. BBX19 interacts with CONSTANS to repress
650 *FLOWERING LOCUS T* transcription, defining a flowering time checkpoint in Arabidopsis. *Plant*
651 *Cell* **26**: 3589-3602.
652 Wang H, Pan J, Li Y, Lou D, Hu Y, Yu D. 2016. The DELLA-CONSTANS transcription factor cascade
653 integrates gibberellic acid and photoperiod signaling to regulate flowering. *Plant Physiol* **172**:
654 479-488.
655 Wang W, Yang D, Feldmann KA. 2011. EFO1 and EFO2, encoding putative WD-domain proteins, have
656 overlapping and distinct roles in the regulation of vegetative development and flowering of
657 Arabidopsis. *J Exp Bot* **62**: 1077-1088.
658 Weinig C, Ungerer MC, Dorn LA, Kane NC, Toyonaga Y, Halldorsdottir SS, Mackay TF, Purugganan MD,
659 Schmitt J. 2002. Novel loci control variation in reproductive timing in *Arabidopsis thaliana* in
660 natural environments. *Genetics* **162**: 1875-1884.
661 Wenkel S, Turck F, Singer K, Gissot L, Le Gourrierec J, Samach A, Coupland G. 2006. CONSTANS and the
662 CCAAT box binding complex share a functionally important domain and interact to regulate
663 flowering of Arabidopsis. *Plant Cell* **18**: 2971-2984.
664 Wigge PA, Kim MC, Jaeger KE, Busch W, Schmid M, Lohmann JU, Weigel D. 2005. Integration of spatial
665 and temporal information during floral induction in Arabidopsis. *Science* **309**: 1056-1059.
666 Wilczek AM, Roe JL, Knapp MC, Cooper MD, Lopez-Gallego C, Martin LJ, Muir CD, Sim S, Walker A,
667 Anderson J et al. 2009. Effects of genetic perturbation on seasonal life history plasticity. *Science*
668 **323**: 930-934.
669 Wu FH, Shen SC, Lee LY, Lee SH, Chan MT, Lin CS. 2009. Tape-Arabidopsis Sandwich - a simpler
670 Arabidopsis protoplast isolation method. *Plant Methods* **5**: 16.
671 Xu F, Li T, Xu PB, Li L, Du SS, Lian HL, Yang HQ. 2016. DELLA proteins physically interact with CONSTANS
672 to regulate flowering under long days in Arabidopsis. *FEBS Lett* **590**: 541-549.
673 Yin R, Arongaus AB, Binkert M, Ulm R. 2015. Two distinct domains of the UVR8 photoreceptor interact
674 with COP1 to initiate UV-B signaling in Arabidopsis. *Plant Cell* **27**: 202-213.
675 Yin R, Messner B, Faus-Kessler T, Hoffmann T, Schwab W, Hajirezaei MR, von Saint Paul V, Heller W,
676 Schaffner AR. 2012. Feedback inhibition of the general phenylpropanoid and flavonol
677 biosynthetic pathways upon a compromised flavonol-3-O-glycosylation. *J Exp Bot* **63**: 2465-2478.
678 Yoo SK, Chung KS, Kim J, Lee JH, Hong SM, Yoo SJ, Yoo SY, Lee JS, Ahn JH. 2005. *CONSTANS* activates
679 *SUPPRESSOR OF OVEREXPRESSION OF CONSTANS 1* through *FLOWERING LOCUS T* to promote
680 flowering in Arabidopsis. *Plant Physiol* **139**: 770-778.
681 Zhang B, Wang L, Zeng L, Zhang C, Ma H. 2015. Arabidopsis TOE proteins convey a photoperiodic signal
682 to antagonize CONSTANS and regulate flowering time. *Genes Dev* **29**: 975-987.

683 Zuo Z, Liu H, Liu B, Liu X, Lin C. 2011. Blue light-dependent interaction of CRY2 with SPA1 regulates COP1
684 activity and floral initiation in Arabidopsis. *Curr Biol* **21**: 841-847.

685

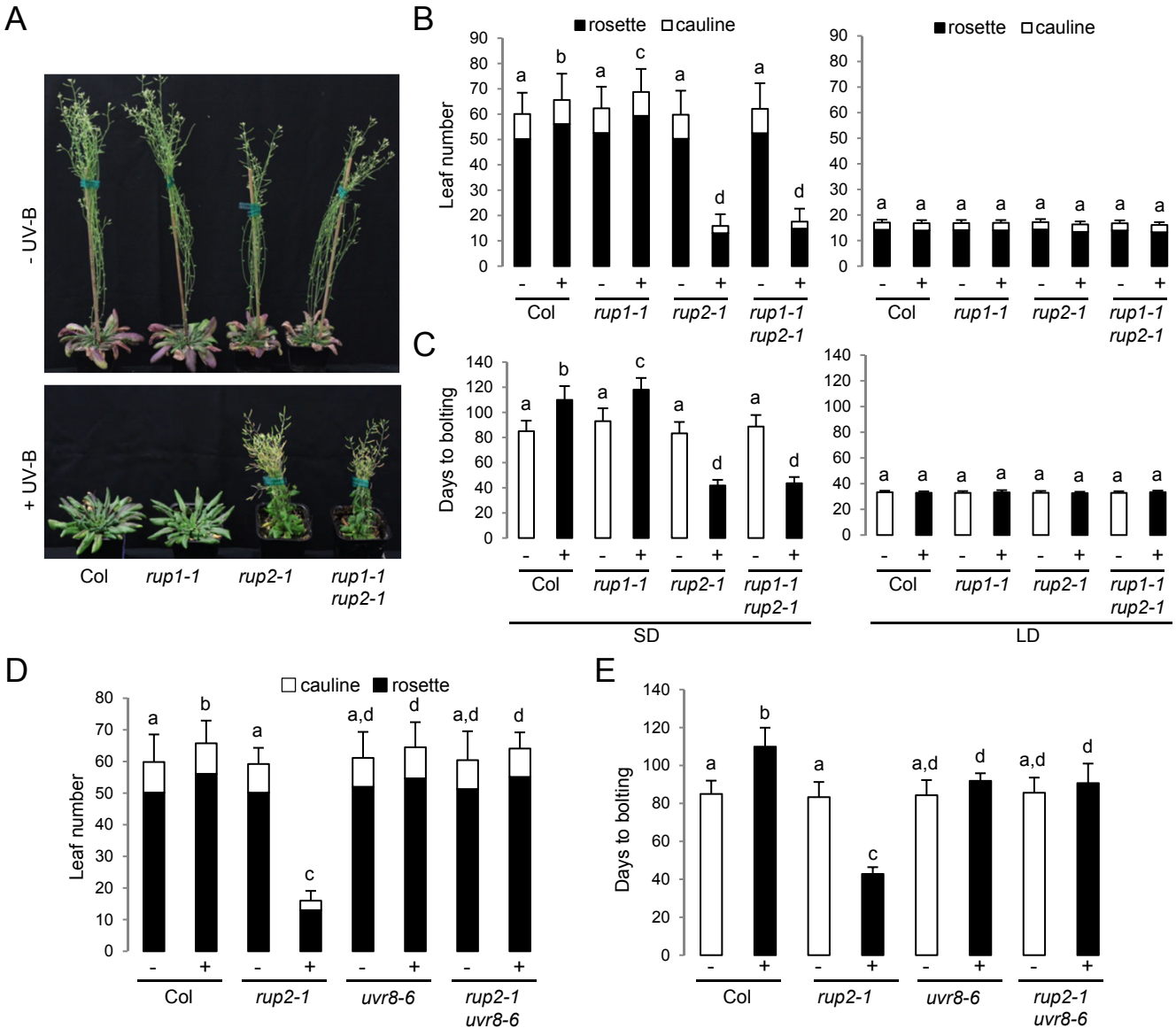

Figure 1. *rup2* flowers early in SD with UV-B, which is dependent on the UVR8 photoreceptor. (*A*) Representative images of 100-d-old wild-type (Col), *rup1-1*, *rup2-1*, and *rup1-1 rup2-1 Arabidopsis* plants grown with (+ UV-B) or without (- UV-B) UV-B. (*B*,*C*) Quantification of flowering time of wild-type (Col), *rup1-1*, *rup2-1*, and *rup1-1 rup2-1* plants grown in SD (*left*) and LD (*right*) with (+) or without (-) UV-B. (*D*,*E*) Quantification of flowering time of wild-type (Col), *rup2-1*, *uvr8-6*, and *rup2-1 uvr8-6* plants grown in SD with (+) or without (-) UV-B. The flowering time is represented by total leaf number (rosette and cauline leaves; *B*,*D*) and days to bolting (*C*,*E*). Error bars represent SD (n = 30); shared letters indicate no statistically significant difference in the means ($P > 0.05$).

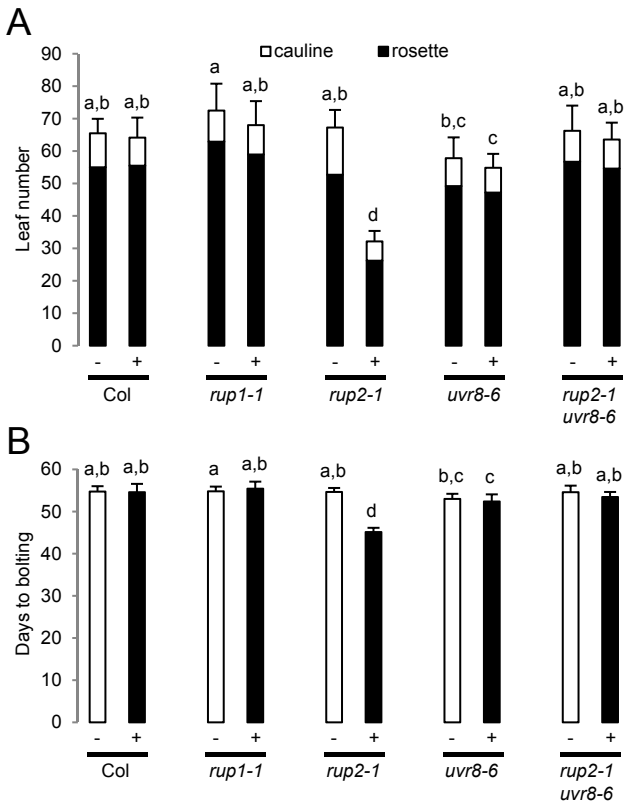

Figure 2. *rup2-1* flowers early under realistic irradiation conditions in a sun simulator. Quantification of flowering time of WT (Col), *rup1-1*, *rup2-1*, *uvr8-6*, and *rup2-1 uvr8-6* plants grown in SD with (+) or without (-) UV. The flowering time is represented by total leaf number (rosette and cauline leaves; *A*) and days to bolting (*B*). Error bars represent SD (n = 20); shared letters indicate no statistically significant difference in the means ($P > 0.05$).

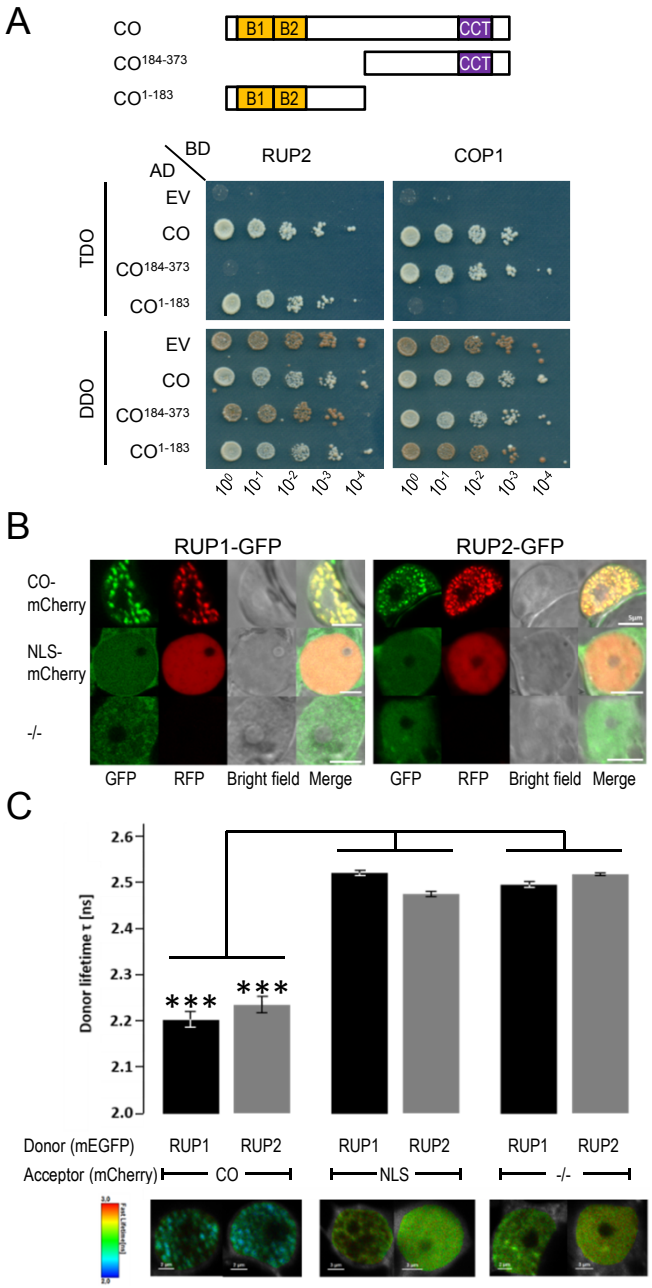

Figure 3. RUP1 and RUP2 interact with CO. (*A*) Interaction of RUP1 and RUP2 with CO in a yeast two-hybrid growth assay. Upper: Schematic representation of full-length and truncated CO used in interaction analysis. Lower: 10-fold serial dilutions of transformed yeast spotted on DDO (nonselective for interaction) and TDO (selective) plates. AD: activation domain; BD: binding domain; EV: empty vector; DDO, SD/-Trp/-Leu; TDO, SD/-Trp/-Leu/-His. (*B*) Co-localization analysis of RUP1-mEGFP and RUP2-mEGFP with either CO-mCherry, NLS-mCherry, or without a mCherry fusion protein (-/-) in transiently transformed *N. benthamiana* epidermal leaf cells. Shown are confocal images in the GFP and RFP channel as well as the corresponding bright field and merged images. White bars = 5 µm. (*C*) FLIM analyses comparing the different FRET pairs. Upper: FLIM measurements of transiently transformed *N. benthamiana* epidermal leaf cells expressing RUP1-mEGFP or RUP2-mEGFP donors in the presence of CO-mCherry, NLS-mCherry acceptor fusion, or without a mCherry acceptor (-/-). Error bars indicate standard deviation ($n \geq 20$); *** indicates a significant difference ($P \leq 0.001$). Lower: Heat maps of representative nuclei used for FLIM measurements. Donor lifetimes of RUP1-mEGFP and RUP2-mEGFP are color-coded according to the scale on the left.

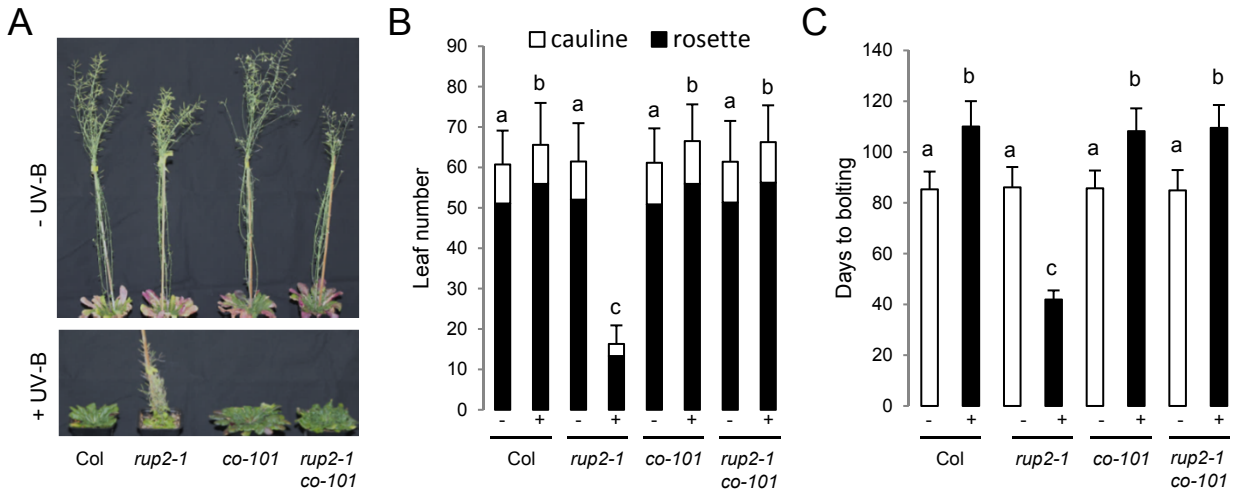

Figure 4. Early flowering of *rup2* in SD supplemented with UV-B depends on the key flowering regulator CO. (*A*) Representative images of 100-d-old wild-type (Col), *rup2-1*, *co-101*, and *rup2-1 co-101 Arabidopsis* plants grown with (+UV-B) or without (-UV-B) UV-B. (*B*,*C*) Quantification of flowering time of wild-type (Col), *rup2-1*, *co-101*, and *rup2-1 co-101* plants grown in SD with (+) or without (-) UV-B. The flowering time is represented by total leaf number (rosette and cauline leaves; *B*) and days to bolting (*C*). Error bars represent SD (n = 21); shared letters indicate no statistically significant difference in the means ($P > 0.05$).

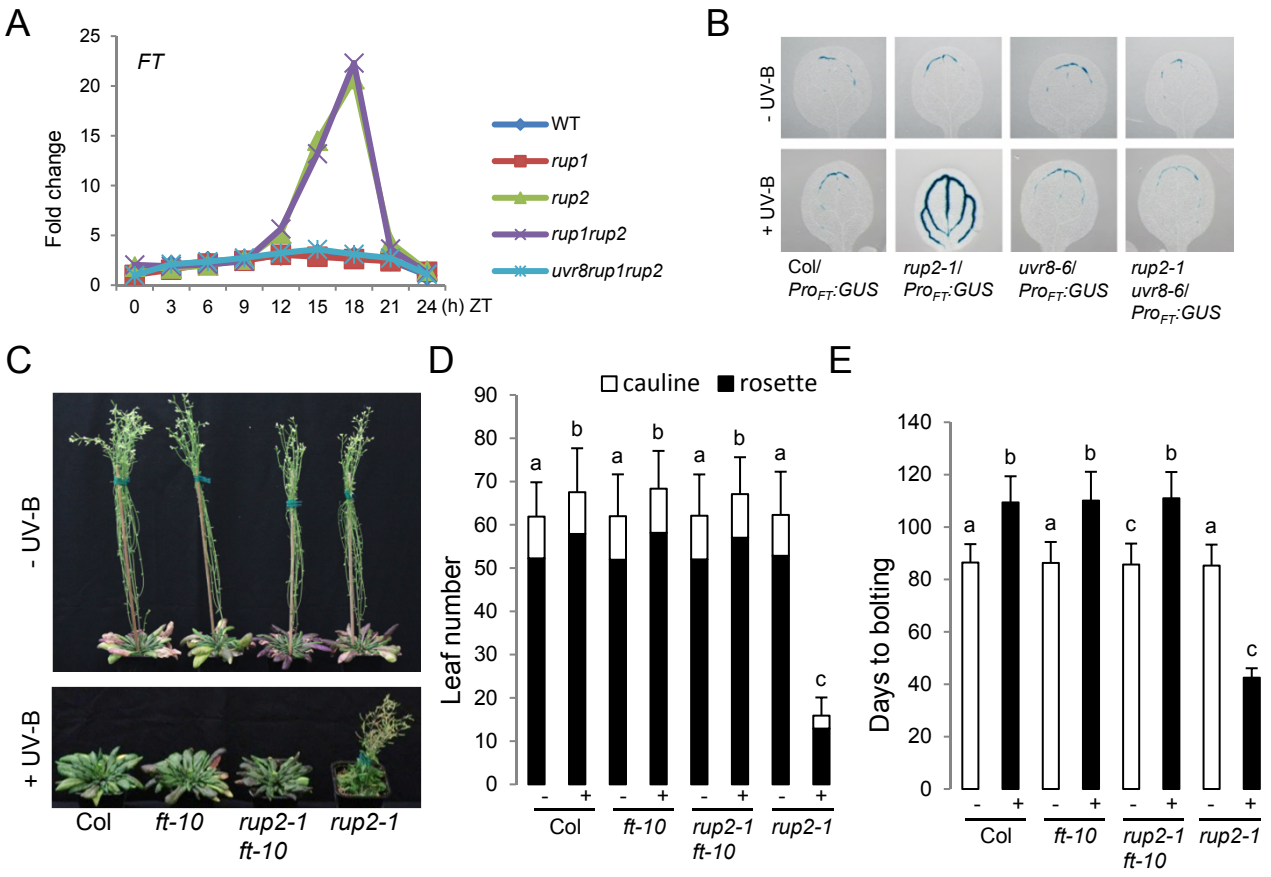

Figure 5. Early flowering of *rup2* in SD with UV-B depends on the florigen FT. (*A*) qRT-PCR analysis of *FT* expression in 30-d-old wild-type, *rup1-1*, *rup2-1*, *rup1-1 rup2-1*, and *uvr8-6 rup1-1 rup2-1* plants grown under SD+UV on soil. Samples were collected every 3 h; a representative experiment is shown. ZT: Zeitgeber time (ZT0 = lights on, ZT8 = lights off). (*B*) GUS assays representing *FT* promoter activity in 5-d-old WT (Col/Pro_{FT}:*GUS*), *rup2-1*/Pro_{FT}:*GUS, uvr8-6*/Pro_{FT}:*GUS*, and *rup2-1 uvr8-6*/Pro_{FT}:*GUS* seedlings grown in SD with (+UV-B) or without (-UV-B) UV-B. (*C*) Representative images of 100-d-old wild-type (Col), *ft-10*, *rup2-1 ft-10* and *rup2-1 Arabidopsis* plants grown with UV-B (+ UV-B), or without (- UV-B). (*D*,*E*) Quantification of flowering time of wild-type (Col), *ft-10*, *rup2-1 ft-10*, and *rup2-1* plants grown in SD with (+) or without (-) UV-B. The flowering time is represented by total leaf number (rosette and cauline leaves; *D*) and days to bolting (*E*). Error bars represent SD (n = 21); shared letters indicate no statistically significant difference in the means ($P > 0.05$).

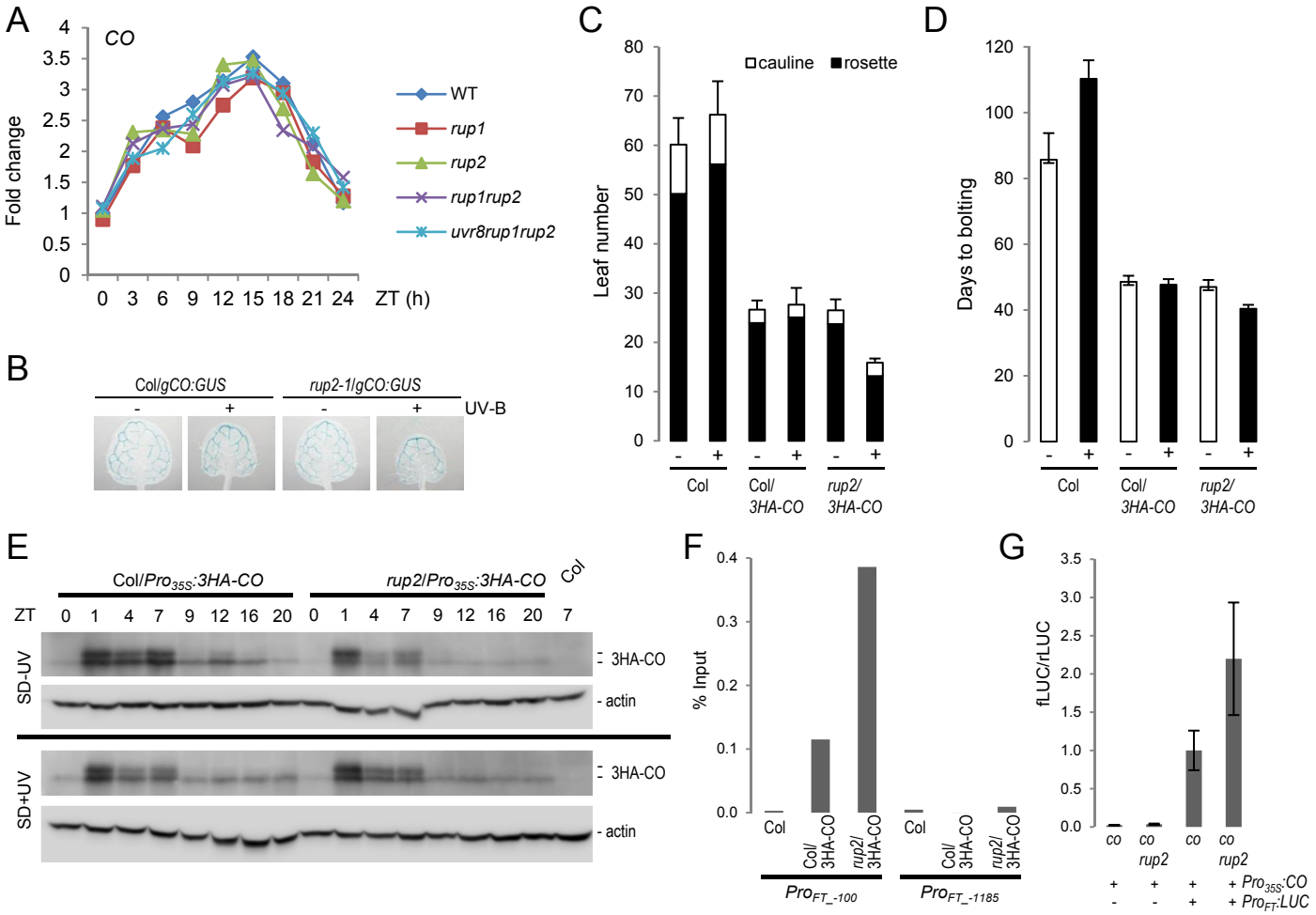

Figure 6. RUP2 represses CO binding to the *FT* promoter and inhibits CO-mediated *FT* expression. (*A*) qRT-PCR analysis of *CO* expression in 30-d-old wild-type, *rup1-1*, *rup2-1*, *rup1-1 rup2-1*, and *uvr8-6 rup1-1 rup2-1* plants grown under SD+UV on soil. Samples were collected every 3 h; a representative experiment is shown. ZT: Zeitgeber time (ZT0 = lights on, ZT8 = lights off). (*B*) GUS assays representing *CO* promoter activity in 5-d-old WT (Col/*gCO:GUS*) and *rup2-1*/*gCO:GUS* seedlings grown in SD with (+ UV-B) or without (- UV-B) UV-B. (*C*,*D*) Quantification of flowering time of WT (Col), Col/Pro_{35S}*:3HA-CO*, and *rup2-1*/Pro_{35S}*:3HA-CO* plants grown in SD with (+) or without (-) UV-B. The flowering time is represented by total leaf number (rosette and cauline leaves; *C*) and days to bolting (*D*). Error bars represent SD (n = 16). (*E*) RUP2 does not affect the diurnal regulation of CO stability in Pro_{35S}*:3HA-CO* overexpression lines. Immunoblot analysis of 3HA-CO protein level at the indicated Zeitgeber time (ZT) in 10-d-old Col/Pro_{35S}*:3HA-CO* and *rup2*/Pro_{35S}*:3HA-CO* plants grown in the absence (SD-UV, upper panel) or presence (SD+UV, lower panel) of UV-B. Actin levels are shown as a loading control; WT (Col) at ZT7 is added as a control sample for anti-HA specificity. (*F*) HA-CO ChIP-qPCR using 12-d-old wild-type (Col), Col/Pro_{35S}*:3HA-CO*, and *rup2*/Pro_{35S}*:3HA-CO* seedlings grown in SD+UV (ZT8). The numbers of the analyzed DNA fragments indicate the positions of the 5′ base pair of the amplicon relative to the translation start site. ChIP efficiency of DNA associated with HA-CO is presented as the percentage recovered from the total input DNA (% Input). (*G*) Relative LUC activity of protoplast isolated from *co-101* and *co-101 rup2-1* plants growing under SD+UV. After protoplast transfection with Pro_{FT}*:fLUC* and Pro_{35S}*:CO*, chemiluminescence was measured at ZT 3–4. Error bars represent SD of three technical replicates.